J Opt
https://doi.org/10.1007/s12596-022-01040-6

RESEARCH ARTICLE

Efficient algorithms for compression and classification of brain tumor images

Fatma M. Ghamry[1,5] · Heba M. Emara[1] · Ahmed Hagag[2] · Walid El-Shafai[1,6] · Ghada M. El-Banby[3] · Moawad I. Dessouky[1] · Adel S. El-Fishawy[1] · Noha A. El-Hag[4] · Fathi E. Abd El-Samie[1,7]

Received: 24 October 2022 / Accepted: 29 November 2022

Abstract Brain tumor is an abnormal cell population that occurs in the brain. Currently, medical imaging techniques play a vital role in brain tumor diagnosis and classification. Brain tumor classification based on Magnetic Resonance Imaging (MRI) has become a promising research area in the field of medical imaging systems. In the brain image, the size of the tumor may vary from patient to patient along with the minute details of the tumor. It is a difficult task for radiologists to diagnose and classify tumors from numerous images. An efficient algorithm is proposed in this paper for tumor classification based on Deep Learning (DL) models. This paper presents three different Convolutional Neural Network (CNN) models for classification of brain tumors. These models are AlexNet, VGG16, and ResNet50. As brain images need to be stored for a along time for research and medical causes, image compression is an efficient tool for minimizing storage space, and also for allowing the deep analysis of brain images. This study depends on a lossy compression method, namely JPEG2000, for the storage of medical brain images. Classification is applied on the dataset with and without compression to estimate the effect of the compression method on the classification performance. Results of the classification models show that ResNet50 achieves a 99.97% accuracy, then VGG16 reaches a 98.83% accuracy, and finally, AlexNet gives a 92.92% accuracy without compression. The compression process is applied with four different compression ratios of 50, 25, 12.5, and 10%. The reduction in accuracy of classification with compression is small, as ResNet50 gives a 98.56% accuracy, and VGG16 gives a 92.92% accuracy, while AlexNet gives an 83.83% accuracy.

Keywords Brain tumor · MRI · Deep Learning (DL) · AlexNet · VGG16 · ResNet50 · Image compression

✉ Noha A. El-Hag
nohaeng940@yahoo.com

1 Department of Electronics and Electrical Communications Engineering, Faculty of Electronic Engineering, Menoufia University, Menouf 32952, Egypt

2 Department of Scientific Computing, Faculty of Computers and Artificial Intelligence, Benha University, Benha 13518, Egypt

3 Department of Industrial Electronics and Control Engineering, Faculty of Electronic Engineering, Menoufia University, Menouf 32952, Egypt

4 Department of Management of Information Systems, The Higher Institute of Commercial Sciences, Al Mahala Al Kobra, Algarbia 31951, Egypt

5 Bilbeis Higher Institute For EngineeringBHIE, Sharqia, Egypt

6 Security Engineering Laboratory, Computer Science Department, Prince Sultan University, Riyadh 11586, Saudi Arabia

7 Department of Information Technology, Collegeof Computer and Information Sciences, Princess Nourah Bint Abdulrahman University, P.O. Box 84428, Riyadh 11671, Saudi Arabia

Introduction

A brain tumor is produced by a partly-developed irregularity in the brain or principal spine, and it disrupts the normal brain job. Brain tumors can be divided into two kinds: benign and malignant. Benign brain tumors do not include cancer cells, and they develop slowly. They do not extend and typically stay in a unique portion of the brain, but malignant brain tumors include cancer cells and develop fast. They diffuse to additional parts of the brain and spine [1].

Published online: 18 March 2023

A malignant tumor is both dangerous and fatal. The World Health Organization (WHO) has classified brain cancers as grade 1 and 2 low-grade tumors (also recognized as benign tumors) and grade 3 and 4 high-grade tumors (commonly known as malignant tumors) based on brain health behavior [2].

Abnormal and uncontrolled synapses represent a feature of brain tumors that can grow in the skull. These tumors put strain on the brain and have a negative effect on the person's health. According to data from the National Brain Tumor Foundation (NBTF), the death rate from brain tumors has risen by approximately 200% in various countries [3–5]. Early identification and categorization of cancers are critical tasks in biomedical imaging research, since they aid in the development of therapeutic strategies that improve patient survival [6].

Several methods are used to identify brain tumors, including CT scans and EEG signals, but the most powerful and extensively-used method is MRI. It generates interior images of body organs using intense and accurate magnetic fields and radio waves. It is more successful than CT and EEG scanning, because it offers more comprehensive information about the organs inside the body [6].

Significant advancements in medical science have been made in recent years as a result of Artificial Intelligence (AI) and DL. The developed techniques allow specialists to identify diseases simply. This task was previously tedious and time-consuming.

The manual approach for diagnosis is time-consuming and might lead to human mistakes due to the large volumes of data and the different forms of brain tumors. As a consequence, a Computer-Assisted Diagnostic (CAD) system is needed. Deep Convolutional Neural Networks (CNNs), which have been proposed in that field, have made a significant progress in image classification algorithms in recent years [7].

Tumor detection can be considered as one of the most important and crucial aspects in determining the kind of treatment, the treatment process, the treatment success level, and the required follow-up. The CNNs represent one of the best significant and applicable types of DL models in addition to feed-forward neural networks in the field of visual image analysis [8].

Image compression is a strategy for minimizing the irrelevancy and redundancy in medical images. It reduces the dimensions of the image folder without sacrificing quality [9]. More images may be saved on a certain amount of disk space with this compression. It similarly speeds up the transmission of images over the Internet by lowering the transmission time. There are two forms of image compression: lossy and lossless. Lossless compression aims at the preservation of image quality in Picture Archiving and Communication System (PACS), and it helps in closely matching of innovative images after medical image restoration. Lossy compression introduces artifacts, and it is implemented with very low bit rates. Because the superfluous information is totally deleted, the image suffers from some deterioration after reconstruction. Although lossy compression is visually lossless under typical viewing conditions, it allows greater compression ratios compared to lossless compression [10].

The main contributions of this paper are summarized as follows:

(i) Three CNNs are tested to classify medical images (AlexNet, VGG16, ResNet50).
(ii) A lossy compression method is applied on the brain images.
(iii) Compression is applied with four different compression ratios.
(iv) Classification is performed with 3 models after the compression process.
(v) High compression ratios and better performance are achieved after classification.
(vi) The proposed approach provides good results for real-time medical datasets.

Related work

Artificial Intelligence (AI) and DL are largely employed in image processing methods for segmenting, identifying, and classifying magnetic resonance images. The objective is classifying and detecting brain tumors. There have been several studies on brain tumor detection and classification [1].

Several studies discussed brain tumor recognition with DL. Sheikh Basheera et al. [11] suggested a technique for diagnosing brain cancer in which the tumor is first segmented from a magnetic resonance image. Then, it is removed using a stochastic gradient descent algorithm by a pre-trained CNN. Muhammad Sajjad et al. [12] proposed classifying multi-grade cancer tumors by using a data augmentation approach on magnetic resonance images, and then refining them using VGG-19 model that has already been trained.

Ahmet Inar et al. [13] compared the accuracy of the pre-trained ResNet50 model with those of other pre-trained models like GoogleNet, AlexNet, and ResNet50 by eliminating the final 5 layers and replacing them with 8 new layers. The improved ResNet50 model produced good results, with a 97.2 % accuracy.

Jun Cheng et al. [14] devised a tumor categorization approach, which has two stages: offline database construction and online retrieval. Brain tumor images are analyzed sequentially in the offline database phase. Tumor segmentation, feature extraction, and distance metric learning are the

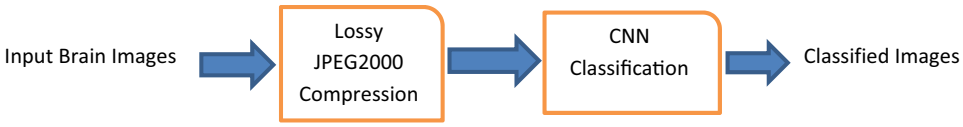

Fig. 1 Proposed classification and compression method

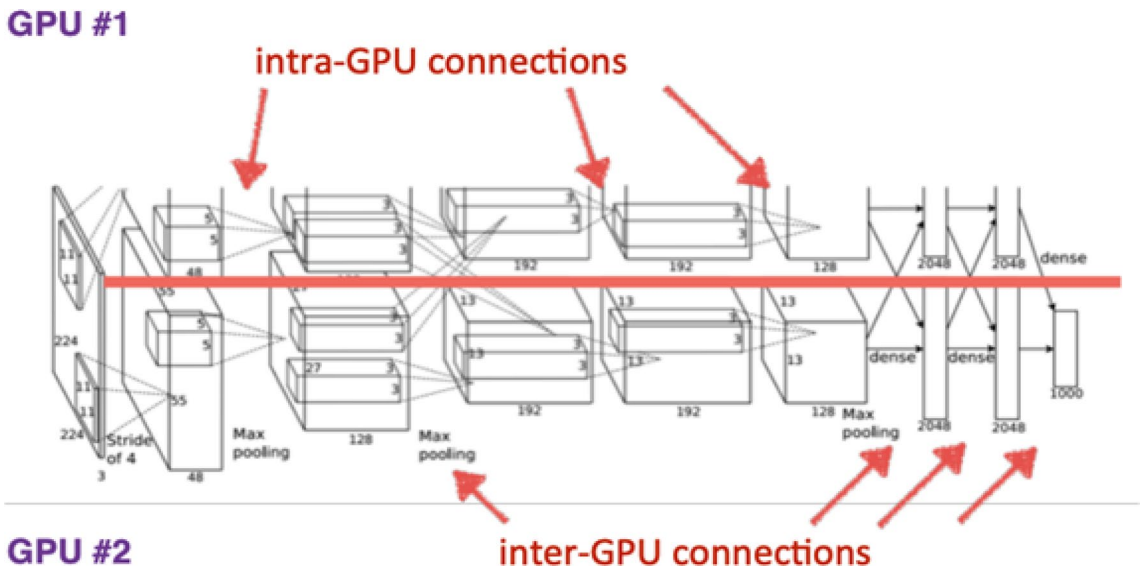

Fig. 2 AlexNet architecture

steps adopted. The input brain images are handled in online learning in a similar manner, and the extracted features are compared according to distance metrics. Although this way does not employ a neural network, it has a classification accuracy of 94.68%.

In recent years, several classification and segmentation approaches have been proposed. Old machine learning [15–18] and new DL models [19–39] have been applied in these strategies. Hemanth et al. [35] presented an approach for MRI brain tumor classification that depends on a modified neural network. To test this approach, 540 magnetic resonance brain images were used. The dataset includes four types of tumors: astrocytoma, meningioma, metastasis, and glioma. The utilized images have 256 × 256 pixels in size. As a pre-processing step, normalization is carried out. The first-order histogram and Gray-Level Co-occurrence Matrix (GLCM) are used to give eight features. This approach produced encouraging results with a sensitivity of 95%, a specificity of 98%, and an accuracy of 98%. Mzoughi et al. (2020) presented a deep multi-scale 3D CNN model for grading of brain tumors from volumetric 3D MRI data. This model correctly classified brain tumor images as high-grade glioma and low-grade glioma with a 96.49% accuracy. For brain tumor classification, Ayadi et al. (2021) proposed a CNN-based Computer-Assisted Diagnosis (CAD) system. Experiments employing the 18-weighted layered CNN model on three different datasets produced a 94.74% classification accuracy for brain tumor category classification and a 90.35% classification accuracy for tumor grading. For brain tumor classification, many researchers used pre-trained CNN models with a transfer learning technique. For example, Cinar and Yildirim (2020) employed a modified form of the pre-trained ResNet50 CNN model for brain tumor detection, replacing the latest 5 layers with 8 additional layers. With this improved CNN model, they were able to obtain a 97.2% accuracy on MRI scans. Khan et al. (2020) used 253 real brain MRI scans with data augmentation to introduce a DL model for classifying brain tumors as cancerous or non-cancerous. They employed edge detection to localize the area of interest in magnetic resonance images before using a basic CNN model to extract the characteristics. They were able to correctly classify 89% of the images [36].

To obtain a high compression ratio, Sevak et al. (2012) employed compressive sensing methods and wavelet coefficients as features to compress medical CT images. The authors obtained a Peak Signal-to-Noise Ratio (PSNR) of 25 dB and a Root Mean Square Error (RMSE) of 14.5 dB [10].

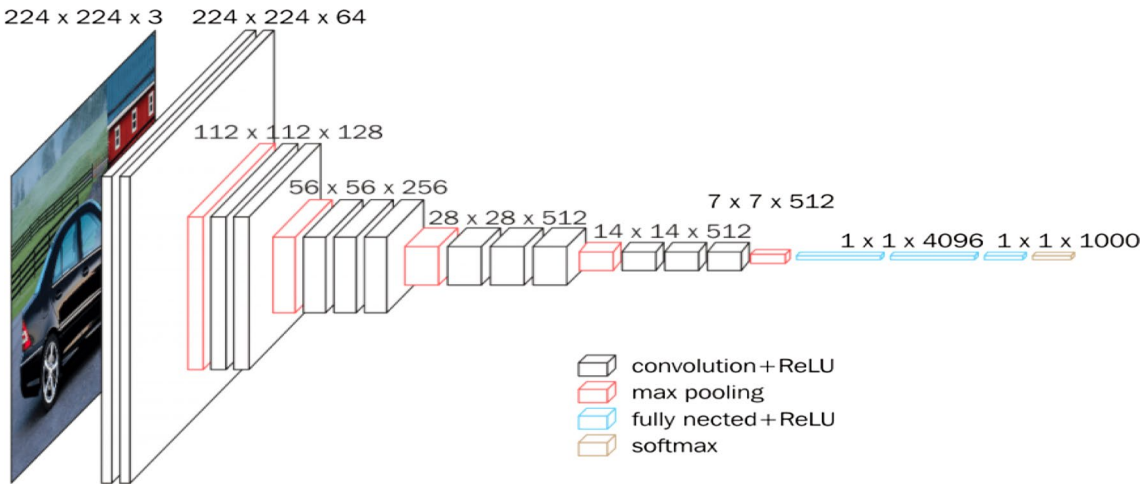

Fig. 3 VGG16 architecture

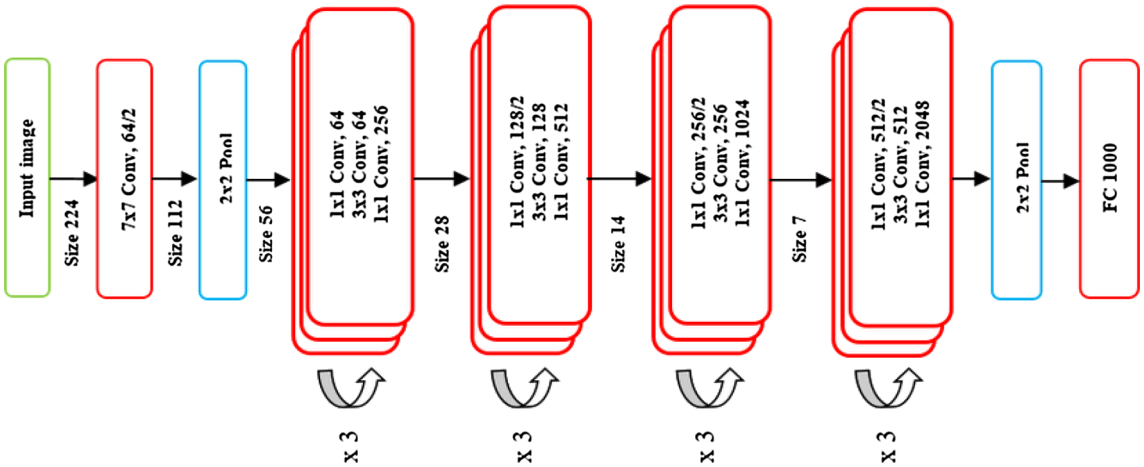

Fig. 4 ResNet50 architecture

Proposed compression and classification approach

The general diagram of the proposed compression and classification approach is revealed in Fig. 1. We classify brain images into two classes with tumor and without tumor after the compression process. The detailed steps of the proposed approach include:

1. The original brain images are classified with three different CNN models: AlexNet, VGG16, and ResNet50 into dual classes containing tumors or not.
2. The same original brain images are compressed by lossy compression using JPEG2000 technique at compression ratios of 50, 25, 12.5 and 10%.
3. All compressed images at four different compression ratios are classified again using the same previous CNN models.
4. A comparison is made between results of classification with and without compression.
5. Results from the comparison reveal the low effect of compression on classification results.

The suggested approach is applied on a dataset of MRI brain tumor images from Kaggle. It consists of two classes of images including tumor, or not. Images are of different dimensions. The first class contains 5504 images for brain with tumors, and the second class contains 6159 images for brain without tumors. All these images from both categories have been used to test the classification with and without compression. The data is available at the link: https://www.kaggle.com/leaderandpiller/brain-tumor-segmentation

Utilized CNN models

- AlexNet model
- VGG16 model
- ResNet50 model

AlexNet model

AlexNet includes 8 layers: 5 convolutional layers, 2 fully-connected layers, and a fully-connected output layer. The size of the input image is 227 × 227. The first convolutional layer employs 96 filters of 11 × 11 window size. In the second convolutional layer, 256 filters are used with a reduced window size of 5 × 5. The window size is 3 × 3 with 384, 384 and 256 filters, in the third, fourth and fifth layers, respectively. The first, second and fifth layers are followed by 3 × 3 max-pooling layers with a stride of 2. Each fully-connected layer has 4096 neurons. Softmax–based classification is employed with 1000 outputs corresponding to the 1000 classes of ImageNet. The network structure is s shown in Fig. 2. Convolutional filters and a nonlinear activation function called ReLU are used in each convolutional layer. To implement feature reduction, the max-pooling layers are needed. Owing to the presence of fully-connected layers, the input size is fixed. The input size is 224 × 224 × 3 in most places; however, owing to padding, it is actually 227 × 227 × 3. AlexNet contains a total of 60 million parameters.

Model Specifications.

The winning model was fine-tuned to include the following features:

- ReLU is used as an activation function.
- Normalization layers are used.
- A 128-piece batch is used.
- The Stochastic Gradient Descent (SGD) momentum algorithm is used as a learning algorithm.
- Extensive data augmentation is adopted with tools including flipping, jittering, cropping, color correction, and other techniques.
- Model assembly is used to achieve the best outcomes.

Max-pooling is used to downsample an image or a representation. The feature map dimensions are reduced by enabling assumptions to be made about the characteristics included in the binned sub-regions.

Overlapping max-pooling layers resemble max-pooling layers, with the exception that the neighboring windows over which the maximum is determined overlap.

The overlapping max-pooling layers, which we will discuss next, come after the first two convolutional layers. Direct connections exist among the third, fourth, and fifth convolutional layers. The second fully-connected layer sends 1000 class labels into a softmax classifier [34].

After all convolutional and fully-connected layers, ReLU nonlinearity is applied. Before pooling, the first and second convolutional layers' ReLU nonlinearity is tailed by a local normalizing step [37].

- VGG16 model

  The VGG16 model includes 16 layers as shown in Fig. 3. Starting by five blocks of convolutional layers, the VGG16 architecture is charted by three fully-connected layers. To guarantee that every activation map keeps the identical spatial sizes as that of the preceding layer, convolutional layers have 3 × 3 kernels with a step of 1 and a packing of 1. In order to minimize the spatial dimensions, a ReLU activation is used after every convolution, and a max-pooling process is used at the conclusion of all blocks. On the way to ensure that each spatial size of the activation map from the earlier layer is split to half, max-pooling layers have 2 × 2 kernels with a stride of 2 and no padding. Before the final 1000-unit fully-connected softmax layer, dual fully-connected layers with 4096 ReLU units are employed [43]. The VGG16 model has the disadvantage of being costly [38].
- ResNet50 model

  We suggest using ResNet50 (residual CNN with 50 layers) to classify brain images in order to aid in the early detection of tumors. In this regard, we use the transfer learning approach to fine-tune the network parameters and hyperparameters of the powerful ResNet50 CNN [39].

  This is performed by preprocessing of the obtained dataset (brain tumor images) and generating a ResNet50 model with pre-determined parameters. MATLAB is used to do this task. Figure 4 shows an illustration of this module [39].
- Convolution through a kernel size of 7 × 7 and 64 different kernels, each having a stride size of 2, is used within the first layer.
- After that, we have max-pooling with a stride size of 2.
- The following convolution has a 1 × 1 size, with 64 kernels, then a 3 × 3 size with 64 kernels, and finally a 1 × 1 size with 256 kernels. These three layers are repeated three times, providing nine layers in this stage.
- Subsequently, there are 128 kernels of size 1 × 1, followed by 128 kernels of size 3 × 3, and finally 512 kernels of size 1 × 1. This phase is performed in four epochs, leading to 12 layers.
- After that, 256 kernels of size 1 × 1 are used, followed by 256 kernels of size 3 × 3 and 1024 kernels of size 1 × 1, leading to 18 layers.

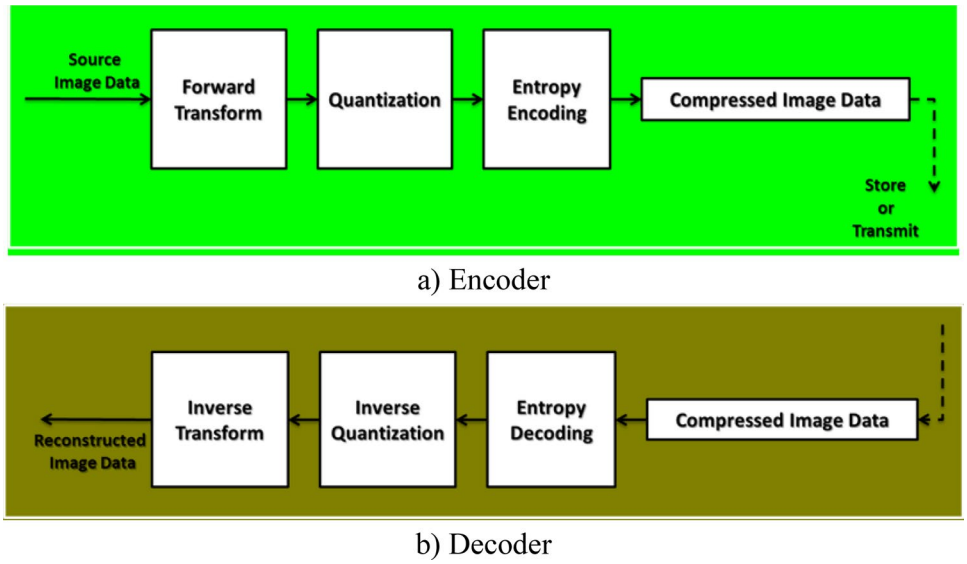

Fig. 5 Block diagram of JPEG2000

- After that, 512 kernels of size 1×1 are added, followed by two additional layers with 512 kernels of size 3×3 and 2048 kernels of size 1×1, leading to nine layers.
- Then, we conduct an average pooling and finish with a fully-conneted layer with 1000 nodes and a softmax function.

Image compression

Brain images with and without tumors can be compressed with lossless or lossy compression. The utilized lossy compression techniques achieve high compression ratios.

- Lossy Compression: Lossy compression can be used to obtain high compression ratios and allow progressive transmission of different types of images. One of the most important features of such techniques is that as more data is supplied, the overall image quality improves steadily.

  Many image compression standards, like JPEG and JPEG2000, have emerged as a result of the development of other compression techniques. They are now widely utilized in several consumer applications. The introduction of compression algorithms based on the wavelet transform followed by bit plane coding, of which Embedded Zero-trees Wavelet (EZW) [40] and Set Partitioning In Hierarchical Trees (SPIHT) [41, 42] are two noteworthy examples, revolutionized the area of still image compression in the mid-90 s.
- SPIHT

  An algorithm that benefits from the Discrete Wavelet Transform (DWT) is the SPIHT [41]. The SPIHT efficacy stems from its ability of subset subdivision and allowance of compact forms of meaning information. Initialization, organizing pass in a List of Insignificant Points (LIP), sorting pass in a List of Insignificant Sets (LIS), and refining pass are the four phases of the SPIHT algorithm. The algorithm first sets the List of Significant Points (LSP) to empty in the initialization stage, and then establishes the roots of similarity trees in the LIP and LIS. The sign bits of the significant coefficients are encoded after every coefficient in the LIP is examined, and the significant coefficients are shifted to the LSP. After that, if an LIS entry is important, a one is transmitted, and its two offspring are verified as if they were LIP entries. A zero is supplied if an LIS entry is unimportant. As a final point, each old LSP entrance is double-checked. A one is sent if it is significantly beneath an existing threshold, and the magnitude is lowered by the present threshold. A zero is sent if the value is unimportant. The original reference [41] has further information about the SPIHT algorithm.

  Two SPIHT compression variants have been presented in [42]. Firstly, a 3-D transform is applied, followed by a basic 3-D SPIHT algorithm. After that, spectral vectors of pixels are vector quantized after a spatial wavelet transform, and a gain-driven SPIHT is utilized.

  Karhunen–Loève Transform (KLT) is utilized to decorrelate the data in the spectral domain [43], and then, a 2-D DCT is used to decorrelate the data in the spatial domain.
- JPEG2000

  The discrete transform is initially applied on the raw image data at the encoder in the JPEG2000 compression engine. Before creating the output bit stream, the

Table 1 Confusion matrix

Name	Positive expected	Negative expected
Positive in nature (1)	(T_p s)	(F_n s)
Negative in nature (0)	($F_p s$)	($T_n s$)

transform coefficients are quantized and entropy coded. To obtain the reconstructed image data, firstly, the code stream is entropy decoded, and then dequantized. After that, it is inverse discrete transformed [44]. The JPEG2000 compression engine is depicted as illustrated in the block diagram of Fig. 5.

The irreversible 9/7 and the reversible 5/3 wavelet transformations have been adopted in JPEG2000. The Cohen–Daubechies–Feauveau 9/7 filter was utilized for spatial decorrelation [41]. As spectral decorrelators, DWT and Principal Component Analysis (PCA) are frequently utilized [42].

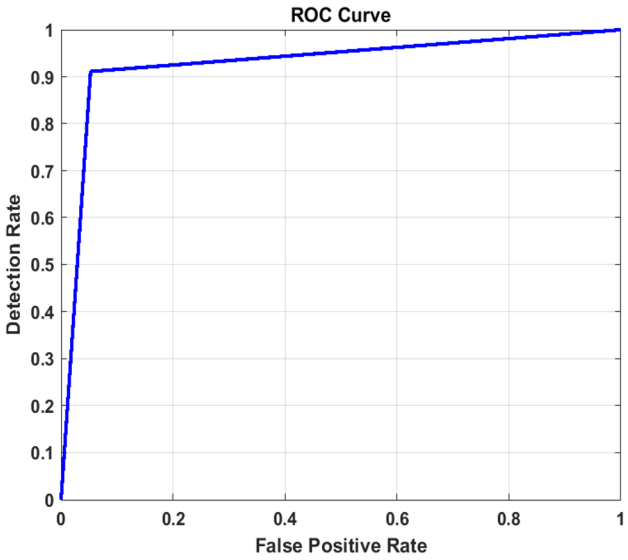

Fig. 7 ROC curve of AlexNet model

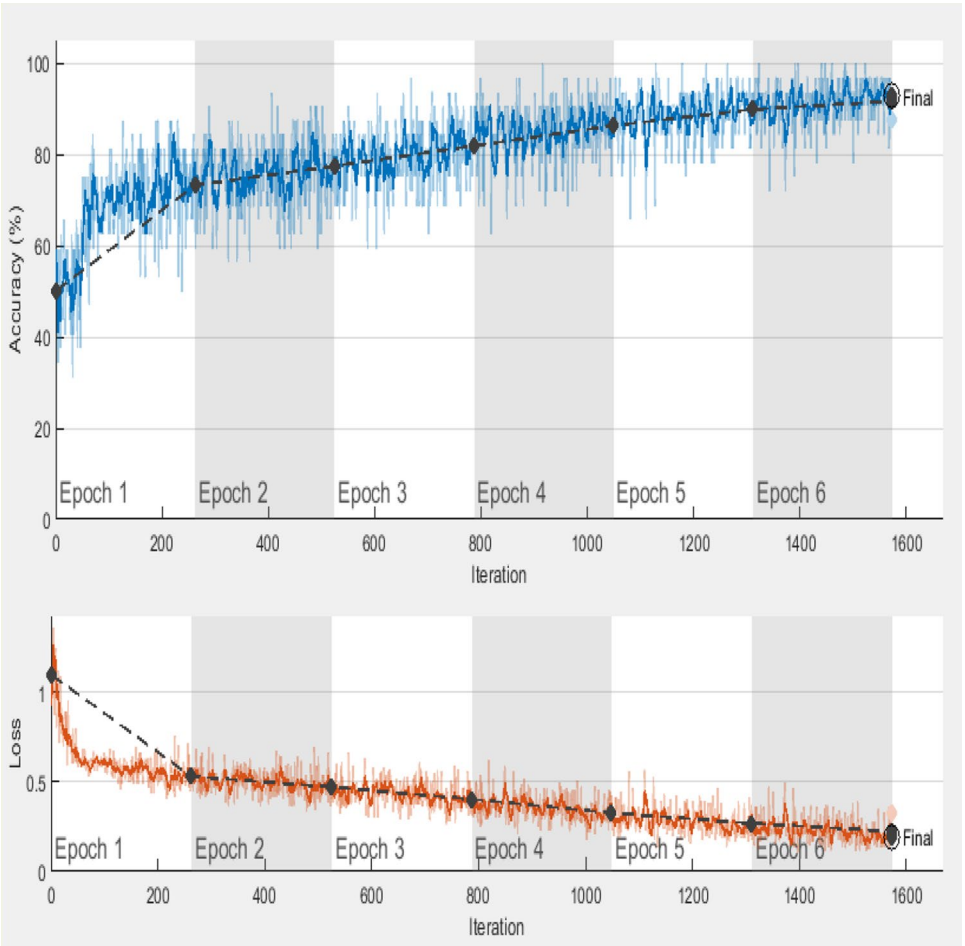

Fig. 6 Accuracy and loss over the number of iterations of AlexNet model

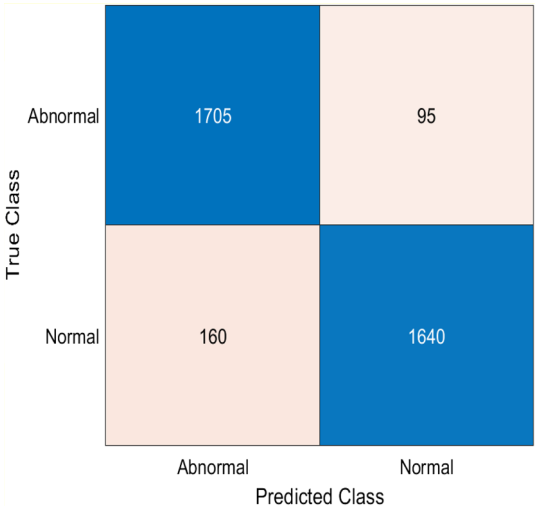

Fig. 8 True classification versus predicted expectation of AlexNet model

Quantization is applied to all coefficients after transformation. This is the process of converting the DWT coefficients into indices to be encoded. The coefficients of each modified tile sub-band are grouped into some rectangular blocks, which are named as code blocks. They are coded one bit plane per a time in the last phase of the encoding process. Every bit plane is managed in three passes. The most significant bit plane has a non-zero element [45].

The outputs are coded by arithmetic methods and combined with comparable passes through other code blocks. The brain images are compressed using JPEG2000 with the PCA spectral decorrelator and the 2-D DWT spatial decorrelator. The authors of [43] implemented JPEG2000 with PCA as a spectral decorrelator.

- Performance Metrics

The confusion matrix contains the different evaluation shown in Table 1. True positive (T_p) refers to the

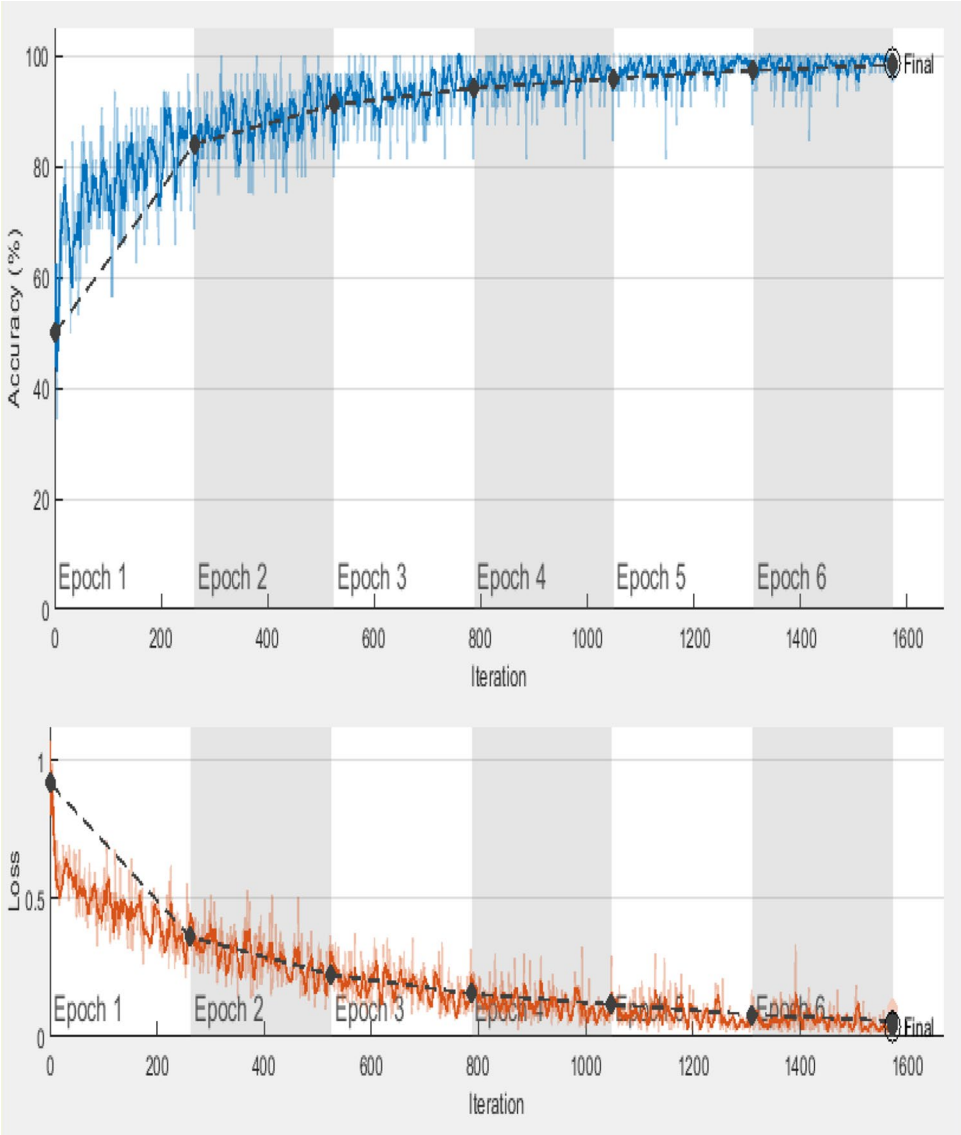

Fig. 9 Percentage accuracy and loss per iteration for VGG16 model

sum of accurately detected abnormal cases [46]. True negative represents the recognized number of accurately detected normal cases (T_n). The normal instances categorized as abnormal diagnoses are referred to as the false positive (F_p). Anomalies that represent the false negative (F_n) are the ones that are observed as normal [47]. The following metrics are used to assess each DL classifier performance. Sensitivity is denoted by (Sen), specificity is identified as ($Spec$), accuracy is represented as (ACC), precision is referred to as ($Preci$), Matthew's Correlation Coefficient is referred to as (MCC). and False Positive Rate is referred to as (FPR). In addition, error, kappa, and F1_score are also used.

Sensitivity is given as follows:

$$Sen = T_p/(F_n + T_p) \tag{1}$$

Specificity is determined as:

$$Spec = \frac{T_n}{F_p + T_n} \tag{2}$$

Accuracy is given as:

$$ACC(\%) = \frac{(T_p + T_n)}{((T_p + T_n) + (F_p + F_n))} \times 100 \tag{3}$$

Precision is given as:

$$Preci = \frac{T_p}{F_p + T_p} \tag{4}$$

Misclassification rate is well-defined as the number of incorrectly categorized labels divided by the number of test images [48]:

Table 2 Results of classification before compression

Model	AlexNet	VGG16	Resnet50
Accuracy (%)	0.9292	0.9883	0.9978
Error (%)	0.0708	0.0117	0.0022
Sensitivity (%)	0.9472	0.9883	0.9989
Specificity (%)	0.9111	0.9883	0.9967
Precision (%)	0.9142	0.9883	0.9967
False Positive Rate (%)	0.0889	0.0117	0.0033
F1_score (%)	0.9304	0.9883	0.9978
Matthew's Correlation Coefficient (%)	0.8589	0.9767	0.9956
Kappa (%)	0.8583	0.9767	0.9956

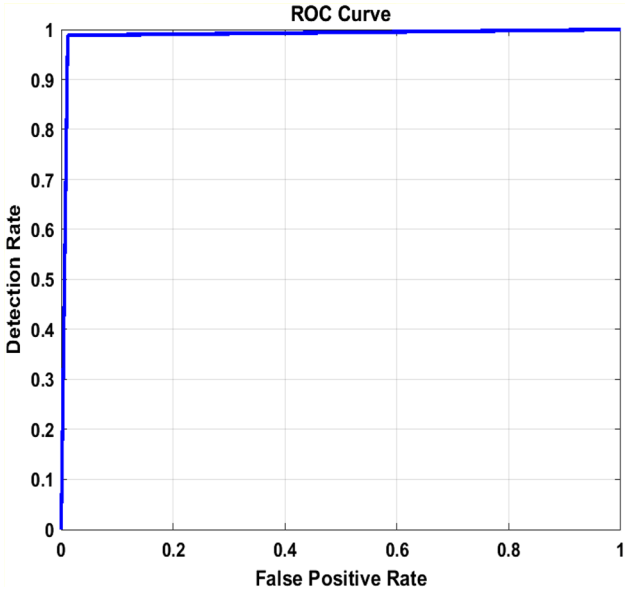

Fig. 10 ROC curve of VGG16 model

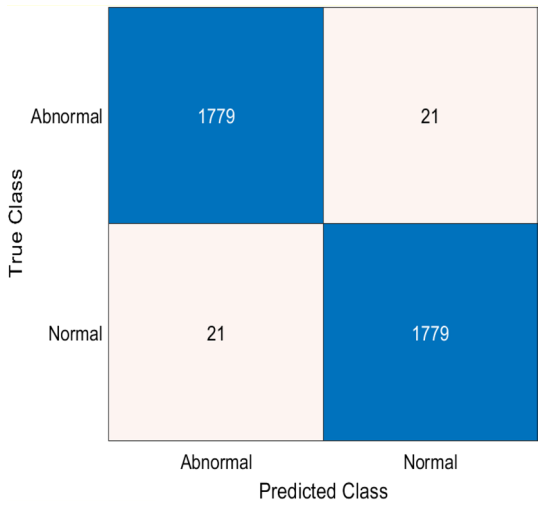

Fig. 11 True classification versus predicted expectation of VGG16 model

$$MCC = \frac{T_n \cdot T_p - F_n \cdot F_p}{\sqrt{(T_p + F_p)(T_p + F_n)(T_n + F_p)(T_n + F_n)}} \tag{5}$$

The false positive rate is specified by:

$$FPR = \frac{F_p}{F_p + T_n} \tag{6}$$

Prevalence represents how often the yes state happens in the example.

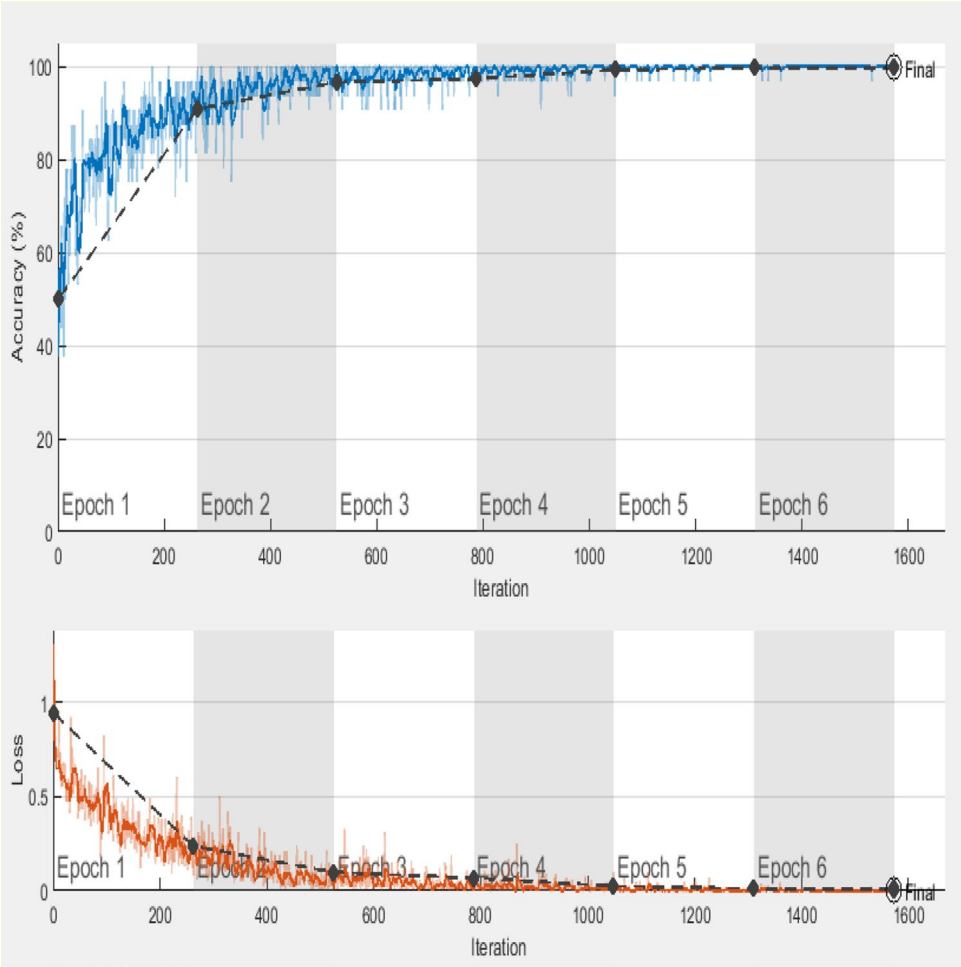

Fig. 12 Accuracy and loss per iteration for ResNet50 model

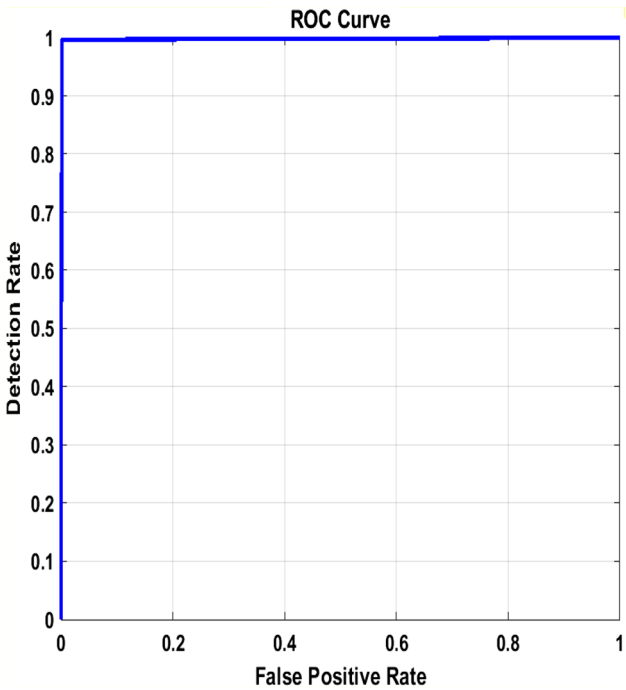

Fig. 13 ROC curve of ResNet50

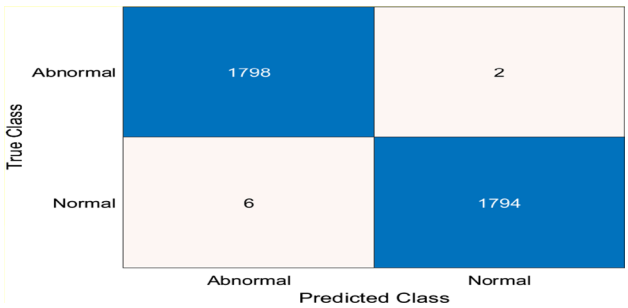

Fig. 14 True classification versus predicted expectation of ResNet50

$$Prev = \frac{F_n + T_p}{(T_p + T_n) + (F_p + F_n)} \tag{7}$$

The F_score, often known as the F_measure, is a measurement of the test accuracy. It is computed by dividing the number of true positives by the total number of positive results (including those that were mistakenly recognized). The recall is the number of genuine positive outputs divided

Table 3 Results for AlexNet after compression with different CRs

Compression ratio	2	4	8	10
Accuracy (%)	0.8322	0.8247	0.8228	0.8367
Error (%)	0.1678	0.1753	0.1772	0.1633
Sensitivity (%)	0.8567	0.7872	0.8233	0.8544
Specificity (%)	0.8078	0.8622	0.8222	0.8189
Precision (%)	0.8167	0.8511	0.8224	0.8251
False Positive Rate (%)	0.1922	0.1378	0.1778	0.1811
F1_score (%)	0.8362	0.8179	0.8229	0.8395
Matthew's Correlation Coefficient (%)	0.6652	0.6513	0.6456	0.6738
Kappa (%)	0.6644	0.6494	0.6456	0.6733

Table 4 Results for VGG16 after compression with different CRs

Compression ratio	2	4	8	10
Accuracy (%)	0.9292	0.8964	0.9275	0.9275
Error (%)	0.0708	0.1036	0.0725	0.0725
Sensitivity (%)	0.9472	0.8961	0.9461	0.9444
Specificity (%)	0.9111	0.8967	0.9089	0.9106
Precision (%)	0.9142	0.8966	0.9122	0.9135
False Positive Rate (%)	0.0889	0.1033	0.0911	0.0894
F1_score (%)	0.9304	0.8964	0.9288	0.9287
Matthew's Correlation Coefficient (%)	0.8589	0.7928	0.8556	0.8555
Kappa (%)	0.8583	0.7928	0.8550	0.8550

Table 5 Results for ResNet50 after compression with different CRs

Compression ratio	2	4	8	10
Accuracy (%)	0.9856	0.9853	0.9750	0.9828
Error (%)	0.0144	0.0147	0.0250	0.0172
Sensitivity (%)	0.9917	0.9944	0.9783	0.9839
Specificity (%)	0.9794	0.9761	0.9717	0.9817
Precision (%)	0.9797	0.9765	0.9719	0.9817
False Positive Rate (%)	0.0206	0.0239	0.0283	0.0183
F1_score (%)	0.9856	0.9854	0.9751	0.9828
Matthew's Correlation Coefficient (%)	0.9712	0.9707	0.9500	0.9656
Kappa (%)	0.9711	0.9706	0.9500	0.9656

by the overall number of samples that have been detected as being positive. The F1_score can be calculated using the harmonic mean of accuracy in addition to the recall [49].

Simulation results

The AlexNet is applied on the brain tumor images of the used datasets.

The results of classification are given in Figs. 6, 7, and 8. In addition, the VGG16 model results are given in Figs. 9, 10, and 11. Moreover, the ResNet50 results are given in Figs. 12, 13, and 14. Finally, the comparison results of the three models are shown in Table 2.

- **Results of classification after compression:**

To certify the success of the suggested algorithm, we test it on the offered dataset images. The basic goal of this proposal is the compression and classification of brain images using lossy compression. The Compression Ratio (CR) is a significant parameter to assess the proposed algorithm. It is estimated based on the compressed image and the original image, and it is defined as the ratio of the size of the compressed image and the size of the source brain image. Tables 3, 4, and 5 show the results of classification of the three models after compression.

Conclusion

In this paper, a brain tumor classification system using CNNs has been introduced to work on compressed images. Three different CNNs models are utilized for image classification to decide if the brain image contains a tumor or not. These models are AlexNet, VGG16, and ResNet50. After compression is done, the images are classified again o investigate the effect of compression on the classification process. ResNet50 has the best efficiency with a 99.78% accuracy. VGG16 comes after with a 98.83% accuracy. AlexNet achieves the lowest accuracy of 92.92%. Compression with ratios of 50, 25, 12.5, and 10% leads to minor effects on the accuracy of classification. On the other hand, image compression is badly needed for minimizing storage space of medical images. The issue that needs to be preserved even with compression is the high ability to analyze and classify medical images. Obviously, from the results, it is clear that the ResNet50 model gives the best accuracy with and without compression.

Acknowledgements The authors would like to thank the Faculty of Electronic Engineering—Menoufia University for the support.

Data availability statements The manuscript does not contain human or animal studies.

Declarations

Conflict of interest The authors declare that they have no conflicts of interest to report regarding the present study.

References

1. H. Khan, W. Jue, M. Mushtaq, M. Umer, Brain tumor classification in MRI image using convolutional neural network. Math. Bio. Eng. **17**, 6203–6216 (2020)
2. NHS, Nat. Hea. Ser.:Brain Tumours, https://www.nhs.uk/conditions/brain-tumours/ (2020).
3. M. AbdEllah, A. Awad, A. Khalaf, H. Hamed, A review on brain tumor diagnosis from MRI images: practical implications, key achievements, and lessons learned. Magnet. Resonance Imag. **61**, 300–318 (2019)
4. T. Logeswari, M. Karnan, An improved implementation of brain tumor detection using segmentation based on hierarchical self-organizing map. Int. J. Comp. **2**(4), p591-598 (2010)
5. M. AbdEllah, A. Awad, A. Khalaf, H. Hamed, "Classification of braintumor MRIs using a kernel support vector machine", 6th Inter. Conf. CCIS. **636**, p151-160 (2016)
6. A. Deshpande, V. Estrela, P. Patavardhanc, The DCT-CNN-ResNet50 architecture to classify brain tumors with super-resolution, convolutional neural network, and the ResNet50. Neur. Inform. **1**, p100013 (2021)
7. W. Ayadi, W. Elhamzi, I. Charfi, M. Atri, Deep CNN for brain tumor classification. Neur Proc Lett **53**, 671–700 (2021)
8. A. Pashaei, H. Sajedi, N. Jazayeri," Brain Tumor Classification via Convolutional Neural Network and Extreme Learning Machines", 8th International Conference, p 25–26(2018)
9. C. Sridhar, P. Pareek, R. Kalidoss, S. Jamal, P. Shukla, S. Nuagah, Optimal medical image size reduction model creation using recurrent neural network and GenPSOWVQ. J. Heal. Eng. **25**, 871 (2022). https://doi.org/10.1155/2022/2354866
10. S. Kumarganesh, M. Suganthi, An Efficient approach for brain image (tissue) compression based on the position of the brain tumor. Imag. Syst. Tech. **26**, 237–242 (2016)
11. S. Basheera, M. Ram, Classification of brain tumors using deep features extracted using CNN. J. Phys. **1172**, 012016 (2019)
12. M. Sajjad, S. Khan, M. Khan, W. Wu, A. Ullah, S. Baik, Multi-grade brain tumor classification using deep CNN with extensive data augmentation. J. Comput Sci. **30**, 174–182 (2019)
13. A. Cinar, M. Yldrm, Detection of tumors on brain MRI images using the hybrid convolutional neural network architecture. Med. Hypo. **139**, 109684 (2020)
14. H. Mohsen, Classification using deep learning neural networks for brain tumors. Fut. Comp. Inform. **1**, 14 (2017)
15. N. Green, S. Chen, A. Hansgen, J. Messenger, B. Groves, J. Carroll, Angiographic views used for percutaneous coronary interventions: a three-dimensional analysis of physician-determined vs. computer-generated views. Cath. Card. Inter. **64**, p451-459 (2005)
16. M. Futrega, A. Milesi, M. Marcinkiewicz, P. Ribalta," Optimized U-Net for Brain Tumor Segmentation", NVID., Sant. Clar. CA,(2021)
17. J. Cheng, W. Huang, S. Cao, R. Yang, W. Yang, Z. Yun, Q. Feng, Enhanced performance of brain tumor classification via tumor region augmentation and partition. PloS ONE **10**(10), 0140381 (2015)
18. M. Ismael, I. Abdel-Qader," Brain tumor classification via statistical features and back-prop- agation neural network", IEEE International Conference Electrical Information Technology (EIT), p 0252–0257 (2018)
19. J. Yu, M. Tan, H. Zhang, D. Tao, Y. Rui, Hierarchical deep click feature prediction for fine- grained image recognition. IEEE Trans. Pat. Anal. Mach. Int. **44**, 563 (2019)
20. J. Yu, J. Li, Z. Yu, Q. Huang, Multimodal transformer with multi-view visual representation for image captioning". IEEE Trans. Circuits Syst. Video Tech. **30**(12), 4467–4480 (2019)
21. J. Yu, J. Yao, J. Zhang, Z. Yu, D. Tao, SPRNet: single-pixel reconstruction for one-stage instance segmentation. IEEE Trans. Cybern. **51**, 1731 (2020)
22. J. Paul, A. Plassard, B. Landman, D. Fabbri," Deep learning for brain tumor classification", Proc. SPIE, (10137), P1–16 (2017)
23. P. Afshar, A. Mohammadi, K. Plataniotis," Brain tumor type classification via capsule networks", 25th IEEE International Conference on Imaging Proceeding (ICIP), p 3129–3133(2018)
24. Y. Zhou, Z. Li,H. Zhu,C. Chen,M. Gao,K. Xu,J. Xu," Holistic brain tumor screening and classification based on densenet and recurrent neural network", Int. Mic. Bra. Spr., p208–217(2018)
25. M. Annamalai, P. Muthiah, An early prediction of tumor in heart by cardiac masses classification in echocardiogram images using robust back propagation neural network classifier. Eng. Tech. Technol. **65**, 52 (2022). https://doi.org/10.1590/1678-4324-2022210316
26. A. Pashaei, Sajedi,N. Jazayeri," Brain tumor classification via convolutional neural network and extreme learning machines", 8th Internationsl Conference on Computer and Knowledge Eng. (ICCKE), p314–319 (2018)
27. N. Abiwinanda, M. Hanif, S.T. Hesaputra, A. Handayani, T.R. Mengko, *Brain tumor classification using convolutional neural network* (Springer, 2019)
28. N. Ghassemi, A. Shoeibi, M. Rouhani, Deep neural network with generative adversarial networks pre-training for brain tumor classification based on MR images". Biomed. Signal Process Control **57**, 101678 (2020)
29. B. Wu, Y. Liu, B. Lang, L. Huang, Dgcnn: disordered graph convolutional neural network based on the gaussian mixture model. Neurocomputing **321**, 346–356 (2018)
30. H. Shi, Y. Zhang, Z. Zhang, N. Ma, X. Zhao, Y. Gao, J. Sun, Hypergraph-induced convolutional networks for visual classification. IEEE Trans. Neural Netw. Syst. **30**(10), 2963–2972 (2018)
31. S. Fu, W. Liu, D. Tao, Y. Zhou, Nie Land HesGCN, "Hessian graph convolutional networks for semi-supervised classification,." Inf. Sci. **514**, 484–498 (2020)
32. S. Fu, W. Liu, Y. Zhou, L. Nie, HpLapGCN: hypergraph p-Laplacian graph convolutional networks. Neurocomputing **362**, 166–174 (2019)
33. N. Khan, U. Chaudhuri, B. Banerjee, S. Chaudhuri, Graph convolutional network for multilabel VHR remote sensing scene recognition. Neurocomputing **357**, 36–46 (2019)
34. F. Sichao, L. Weifeng, L. Shuying, Z. Yicong, Two-order graph convolutional networks for semi-supervised classification". IET Imag. Proc. **13**(14), 2763–2771 (2019)
35. D.J. Hemanth, C. Vijila, A. Selvakumar, J. Anitha, Performance improved iteration-free artificial neural networks for abnormal magnetic resonance brain image classification. Neural Com. **130**, 98–107 (2014)
36. E. Irmak, Multi-classification of brain tumor mri images using deep convolutional neural network with fully optimized framework. Iran J. Sci. Tech., Trans. Electr. Eng. **45**, 1015–1036 (2021)
37. A. Krizhevsky, I. Sutskever, E.G. Hinton, ImageNet classification with deep convolutional neural networks. Commun. ACM **60**, 84 (2012)
38. S. Tammina, Transfer learning using VGG-16 with deep convolutional neural network for classifying images. Sci. Res. Publ. **9**(10), 143 (2019)

39. R.I. Bendjillali, M. Beladgham, K. Merit, A.T. Ahmed, llumination-robust face recognition based on deep convolutional neural networks architectures. Electr. Eng. Computer Sci. **18**, 1015–1027 (2019)
40. J. Shapiro, Embedded image coding using zerotrees of wavelet coefficients. IEEE Trans. Signal Proc. **41**(12), 3445–3462 (1993)
41. A. Said, W. Pearlman, (1996)A new, fast, and efficient image codec based on set partitioning in hierarchical trees. IEEE Trans Circuits Syst Video Technol 6(3): 243–250
42. P. Dragotti, G. Poggi, A. Ragozini, Compression of multispectral images by three-dimensional SPIHT algorithm. IEEE Trans. Geol. Remote Sens. **38**(1), 416–428 (2000)
43. J. Saghri, A. Tescher, J. Reaga, Practical transform coding of multispectral imagery. IEEE Signal Proc. Mag. **12**(1), 32–43 (1995)
44. A. Cohen, I. Daubechies, J. Feauveau, Biorthogonal bases of compactly supported wavelets. Commun. Pure Appl. Math. **45**(5), 485–560 (1992)
45. B. Penna, T. Tillo, E. Magli, G. Olmo, Transform coding techniques for lossy hyperspectral data compression. IEEE Trans. Geol. Remote Sens. **45**(5), 1408–1421 (2007)
46. F. Aulí-Llinàs ," BOI codec",Accessed, p 07–09(2015)
47. https://www.dataschool.io/simple-guide-to-confusion-matrix-terminology
48. M. Shoaib, Deep convolutional neural networks for COVID-19 automatic diagnosis. Micr. Res. Technol. **84**, 2504–2516 (2021)
49. Y. Sasaki,"The truth of the F-measure",YS-26(2007)